Supporting Information

Superior Light Absorbing CdS/Vanadium Sulphide Nanowalls @ TiO_2 Nanorod Ternary Heterojunction Photoanodes for Solar Water Splitting

Soumyajit Maitra, Somoprova Halder, Toulik Maitra, Subhasis Roy*

Department of Chemical Engineering, University of Calcutta, 92 A. P. C. Road, Kolkata 700009, India

*Corresponding author's e-mail address: subhasis1093@gmail.com/ srchemengg@caluniv.ac.in

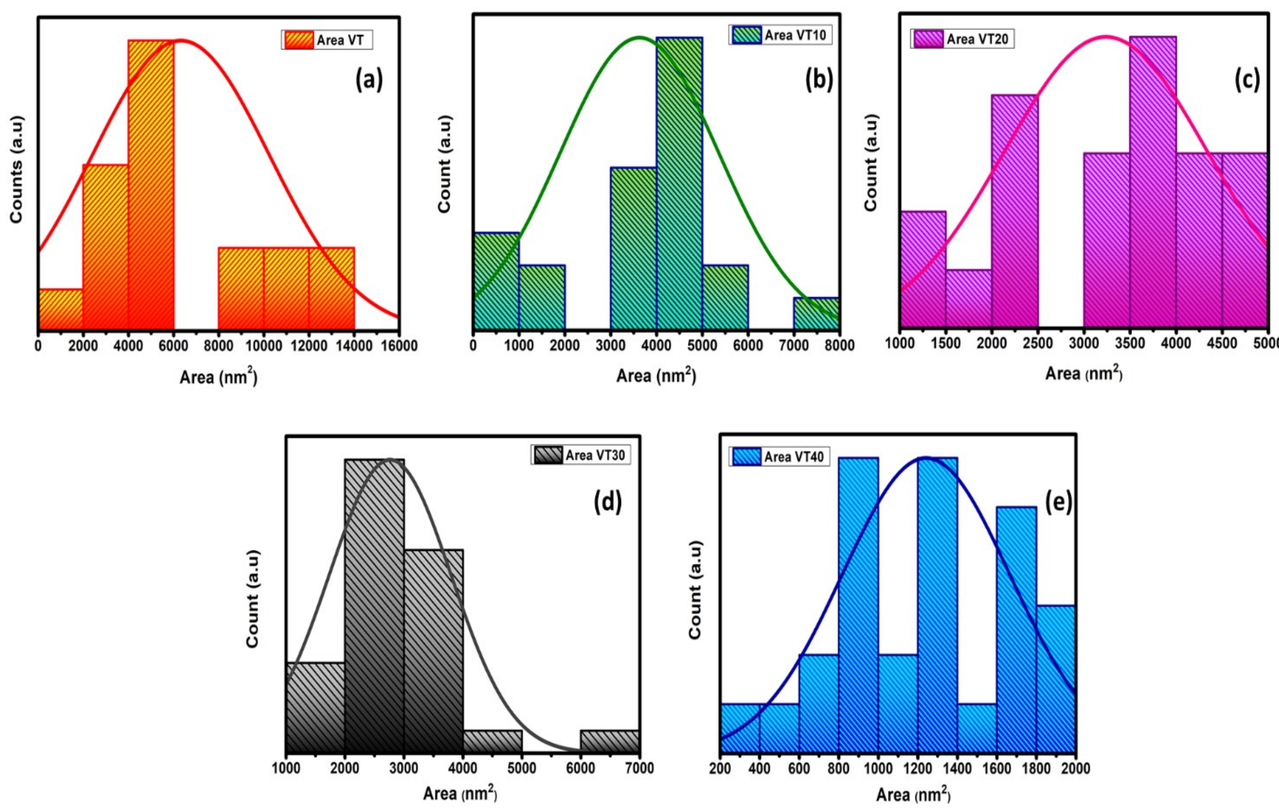

Fig S1. Histogram plots showing the distribution of pore area for samples (a) VT (b) VT10 (c) VT20 (d) VT30 (e) VT40

Histogram plots in Figure S2 shows the change in mean pore area with the gradual increase in CdS loading. There is a clear observable shift towards smaller values of area for the mean value of the distribution with an increase in CdS loading, indicating that extra deposition of CdS reduced the overall pore area, causing a reduction in solvent flux and effective catalytic surface area.

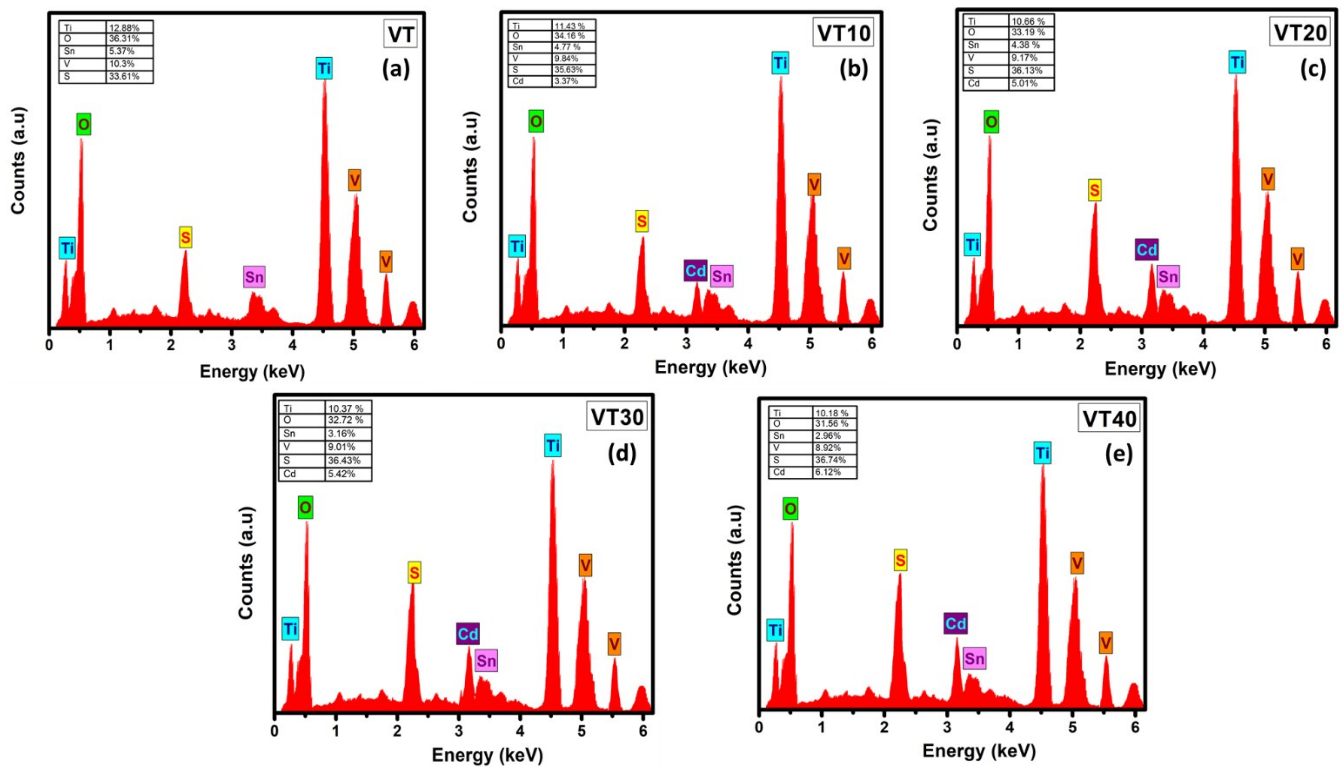

Fig S2 Showing the EDAX plots for the samples (a) VT (b) VT10 (c) VT20 (d) VT30 € VT40

The EDAX plots in fig. S3 shows the presence of Ti, O, V, S present due to the presence of TiO_2 and vanadium sulphide its VS_4 and VS_2 phases. The peaks for Sn are due to the presence of FTO glass substrate. After CdS loading in sample VT10, peaks for Cd appeared with the increase in S peaks gradually with increased cycling of CdS

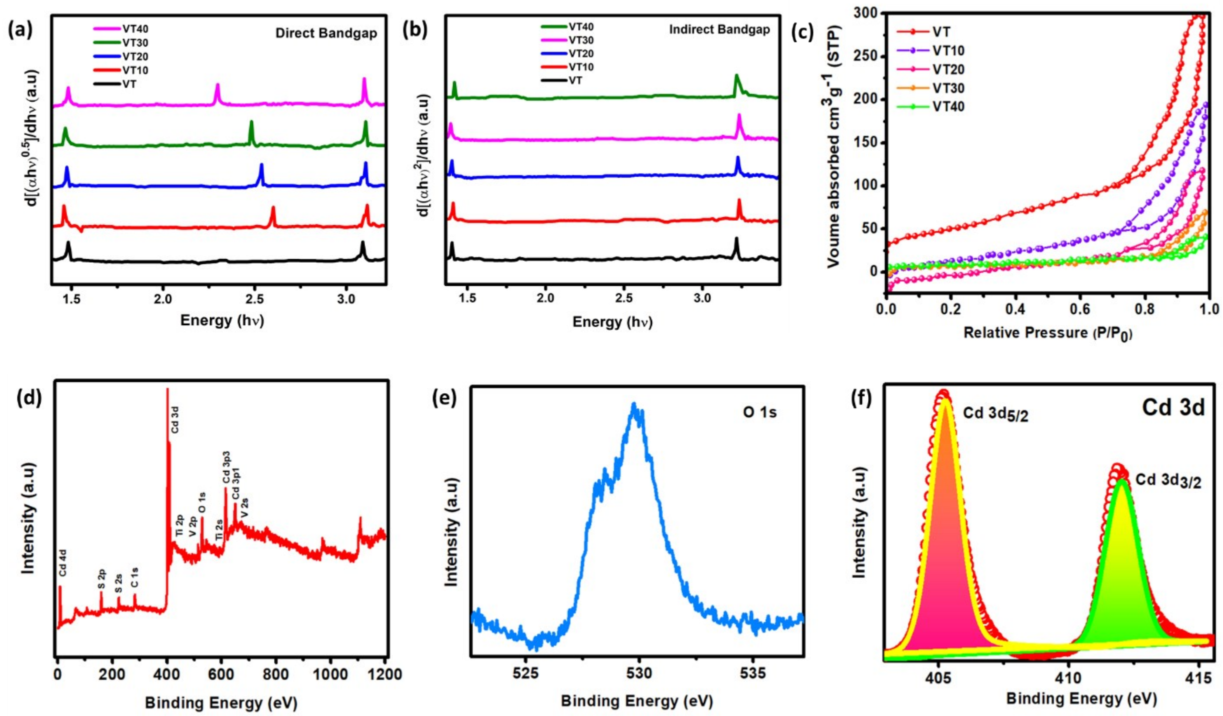

Fig S3. Differential method of bandgap plots of the fabricated photoanodes for (a) Direct bandgap (b) Indirect bandgap (c) BET analysis plots of the fabricated photoanodes (d) XPS surface scan plot of VT20 (e) O 1s Plots (f) Cd 3d plot

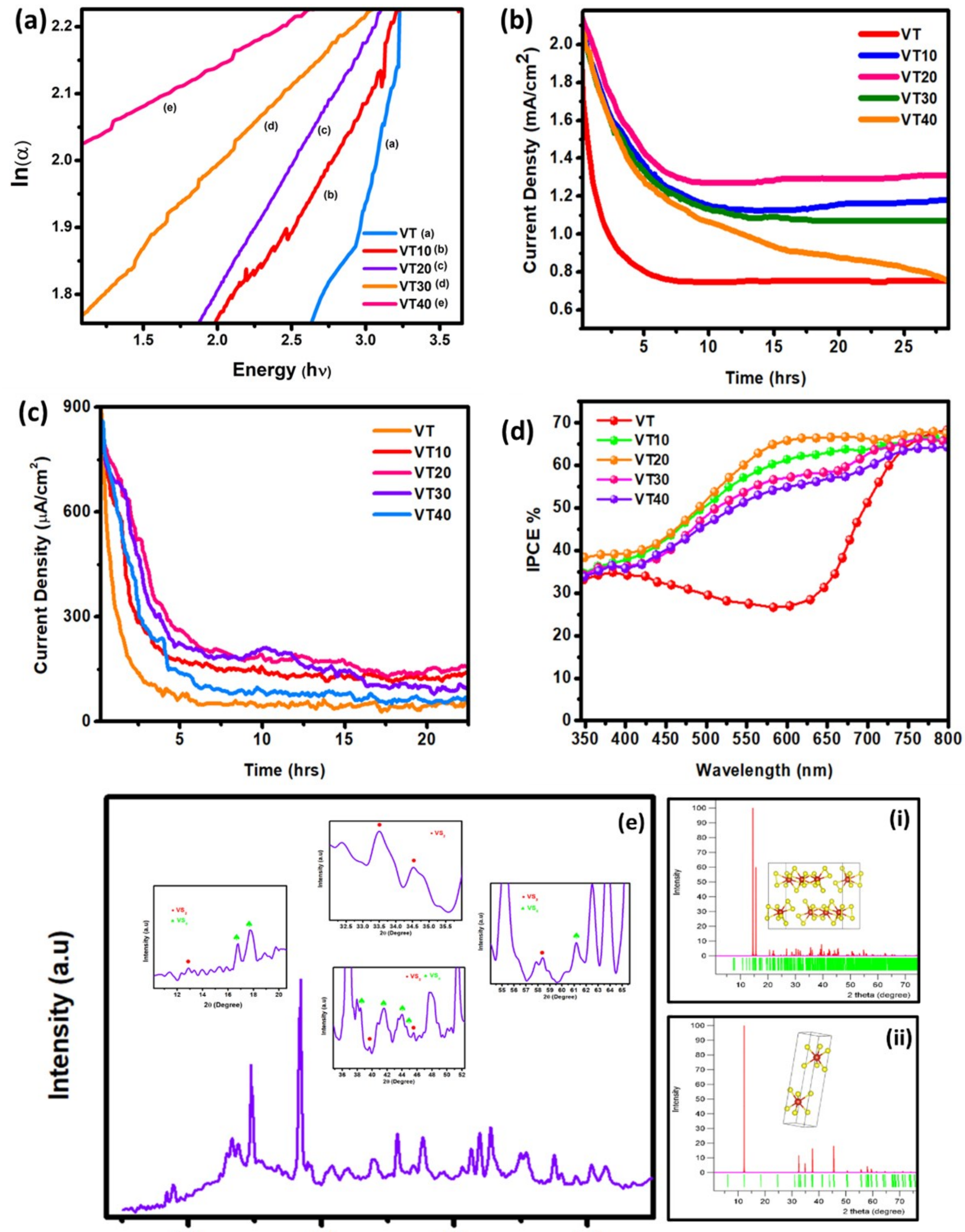

Fig S4. (a) Urbach energy plots for the fabricated photoanodes (b) Chronoamperometry plots for fabricated photoanodes under visible light irradiation (c) Chronoamperometry plots for fabricated photoanodes under UV light irradiation (d) IPCE analysis of the fabricated photoanodes (e) XRD plot of VT20 with magnified peaks of VS 2 and VS 4 in inset (i) Simulated XRD of VS 4 (ii) Simulated

XRD of VS 2 Urbach energy plots demonstrate a gradual decrease in slope with increase in CdS loading indicating that the presence of over deposited CdS with poor morphology and low crystallinity results in formation of shallow low energy tail states acting as recombination centres, thereby reducing photoelectrochemical performance. Chronoamperometry has been carried out using both visible light (fig S4(b)) and UV irradiation (fig S4(c)). IPCE analysis has been carried out as shown in fig S4d. Magnified XRD image along with simulated XRD peaks for VS_2 and VS_4 have been shown in fig S4(e).

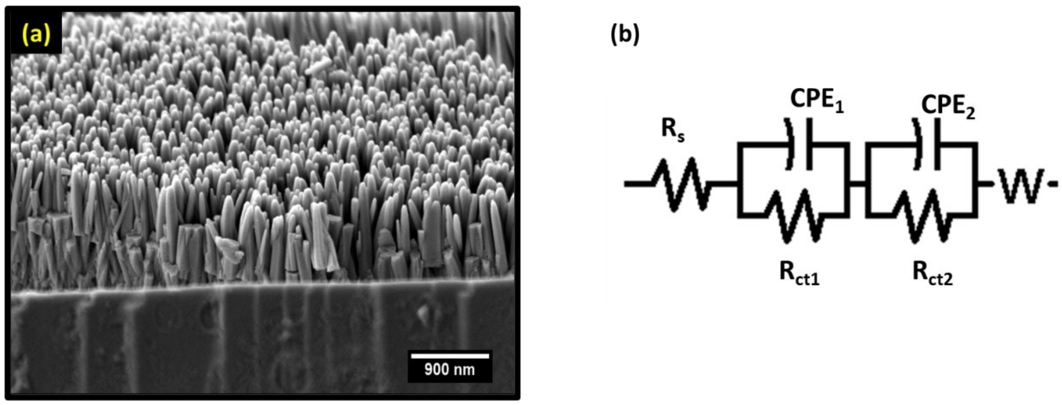

Fig S5. (a) SEM image of pristine TiO_2 nanorods array cross section (b) Randles' Circuit for VT

Fig. S5 shows the SEM images if TiO_2 nanorods grown on FTO glass substrates. The length of the nanorods were approximately 382.7 nm and the diagonal of the top face was approximately 153.4 nm. The Randles circuit for VT has been shown in fig S5b.

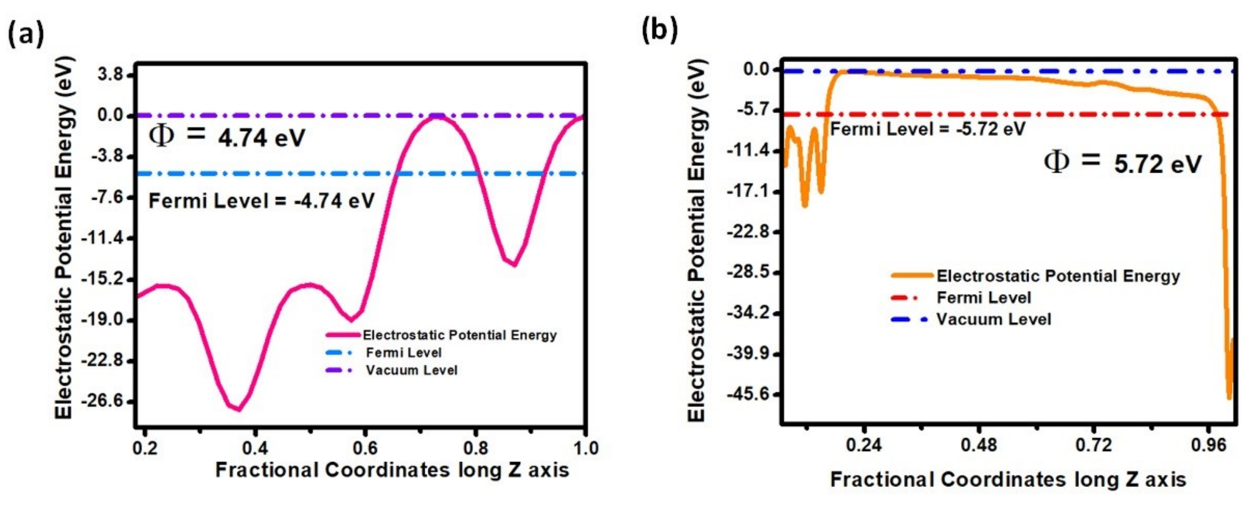

Fig S6. Electrostatic potential energy plots for (a) VS_4/TiO_2 junction (b) CdS/VS_4 junction

Table S1. Computational Details about AFORS-HET band diagram simulation

Parameters	**TiO_2** [4,5,7,9,11]	**VS_4** [2,3,6,8]	**CdS** [1,10,12]
dK **(dielectric constatnt)**	43.2	3.1	5.3
χ (eV) **(absolute elelctronegativity)**	5.81	6.28	5.18
Eg (eV) **(optical bandgap)**	3.2	1.5	2.4
Na **(acceptor level density)**	0	2.1E21	0
Nd **(donor level density)**	1.73E18	0	2.53E18

References:

[1] K.H. Cho, Y.M. Sung, The formation of Z-scheme CdS/CdO nanorods on FTO substrates: The shell thickness effects on the flat band potentials, Nano Energy. 36 (2017) 176–185.

[2] J. Du, C. Xia, W. Xiong, T. Wang, Y. Jia, J. Li, Two-dimensional transition-metal dichalcogenides-based ferromagnetic van der Waals heterostructures, Nanoscale. 9 (2017) 17585–17592.

[3] G. Gogoi, C.T. Moi, A.S. Patra, D. Gogoi, P.N. Rao, M. Qureshi, A Z-Scheme Strategy that Utilizes ZnIn2S4 and Hierarchical VS2 Microflowers with Improved Charge-Carrier Dynamics for Superior Photoelectrochemical Water Oxidation, Chemistry - An Asian Journal. 14 (2019) 4607–4615.

[4] J. Hu, S. Zhang, Y. Cao, H. Wang, H. Yu, F. Peng, Novel Highly Active Anatase/Rutile TiO2 Photocatalyst with Hydrogenated Heterophase Interface Structures for Photoelectrochemical Water Splitting into Hydrogen, ACS Sustainable Chemistry and Engineering. 6 (2018) 10823–10832.

[5] S. Kashiwaya, J. Morasch, V. Streibel, T. Toupance, W. Jaegermann, A. Klein, The Work Function of TiO2, Surfaces. 1 (2018) 73–89.

[6] N. Kishore, V. Nagarajan, R. Chandiramouli, Exploring the structural stability and electronic properties of VS2 nanostructures - A DFT study, Journal of Nano- and Electronic Physics. 9 (2017) 3–6.

[7] R. O'Hayre, M. Nanu, J. Schoonman, A. Goossens, Mott - Schottky and charge-transport analysis of nanoporous titanium dioxide films in air, Journal of Physical Chemistry C. 111 (2007) 4809–4814.

[8] Y. Qu, H. Pan, C.T. Kwok, Z. Wang, Effect of Doping on Hydrogen Evolution Reaction of Vanadium Disulfide Monolayer, Nanoscale Research Letters. 10 (2015) 1–7.

[9] M.C.K. Sellers, E.G. Seebauer, Measurement method for carrier concentration in TiO2 via the Mott-Schottky approach, Thin Solid Films. 519 (2011) 2103–2110.

[10] X. Yong, M.A.A. Schoonen, The absolute energy positions of conduction and valence bands of selected semiconducting minerals, American Mineralogist. 85 (2000) 543–556.

[11] H. Yu, H. Irie, K. Hashimoto, Conduction band energy level control of titanium dioxide: Toward an efficient visible-light-sensitive photocatalyst, Journal of the American Chemical Society. 132 (2010) 6898–6899.

[12] G. Zhang, D. Monllor-Satoca, W. Choi, Band energy levels and compositions of CdS-based solid solution and their relation with photocatalytic activities, Catalysis Science and Technology. 3 (2013) 1790–1797.